

UCSF

UC San Francisco Previously Published Works

Title

Calibrated flux measurements reveal a nanostructure-stimulated transcytotic pathway

Permalink

<https://escholarship.org/uc/item/70r0m3wr>

Journal

Experimental Cell Research, 355(2)

ISSN

0014-4827

Authors

Stewart, Tarianna
Koval, William T
Molina, Samuel A
[et al.](#)

Publication Date

2017-06-01

DOI

10.1016/j.yexcr.2017.03.065

Peer reviewed



Published in final edited form as:

Exp Cell Res. 2017 June 15; 355(2): 153–161. doi:10.1016/j.yexcr.2017.03.065.

Calibrated flux measurements reveal a nanostructure-stimulated transcytotic pathway

Tarianna Stewart^{1,2}, William T. Koval², Samuel A. Molina², Suzanne M. Bock³, James W. Lillard Jr.¹, Russell F. Ross³, Tejal A. Desai⁴, and Michael Koval^{2,5}

¹Morehouse School of Medicine, Atlanta, GA

²Division of Pulmonary Allergy, Critical Care and Sleep Medicine, Department of Medicine, Emory University School of Medicine

³Kimberly-Clark Corporation, Atlanta, Ga

⁴Department of Bioengineering and Therapeutic Sciences, University of California, San Francisco, CA

⁵Department of Cell Biology, Emory University School of Medicine, Atlanta, GA

Abstract

Transport of therapeutic agents across epithelial barriers is an important element in drug delivery. Transepithelial flux is widely used as a measure of transit across an epithelium, however it is most typically employed as a relative as opposed to absolute measure of molecular movement. Here, we have used the calcium switch approach to measure the maximum rate of paracellular flux through unencumbered intercellular junctions as a method to calibrate the flux rates for a series of tracers ranging in 0.6 to 900 kDa in size across barriers composed of human colon epithelial (Caco-2) cells. We then examined the effects of nanostructured films (NSFs) on transepithelial transport. Two different NSF patterns were used, Defined Nanostructure (DN) 2 imprinted on polypropylene (PP) and DN3 imprinted on polyether ether ketone (PEEK). NSFs made direct contact with cells and decreased their barrier function, as measured by transepithelial resistance (TER), however cell viability was not affected. When NSF-induced transepithelial transport of Fab fragment (55 kDa) and IgG (160 kDa) was measured, it was unexpectedly found to be significantly greater than the maximum paracellular rate as predicted using cells cultured in low calcium. These data suggested that NSFs stimulate an active transport pathway, most likely transcytosis, in addition to increasing paracellular flux. Transport of IgG via transcytosis was confirmed by immunofluorescence

*Correspondence and requests for reprints should be addressed to: Michael Koval Emory University School of Medicine, Division of Pulmonary, Allergy, Critical Care and Sleep Medicine, Whitehead Biomedical Research Building, 615 Michael St., Suite 205 Atlanta, GA 30322. Tel.: 404-712-2976. mhkoval@emory.edu.

Publisher's Disclaimer: This is a PDF file of an unedited manuscript that has been accepted for publication. As a service to our customers we are providing this early version of the manuscript. The manuscript will undergo copyediting, typesetting, and review of the resulting proof before it is published in its final citable form. Please note that during the production process errors may be discovered which could affect the content, and all legal disclaimers that apply to the journal pertain.

Declaration of interest

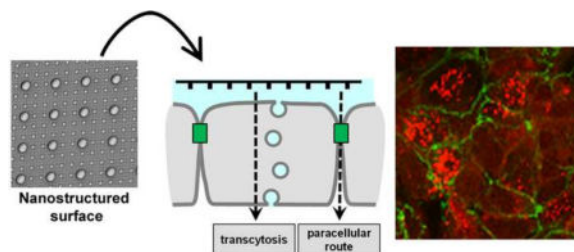
The authors report no conflicts of interest associated with this manuscript.

Author contributions

TS, TAD, RFR, JWJ and MK designed the study. TS, WTK, SAM, SMB and MK conducted the experimental work and data analysis. TS, SAM, JWJ and MK wrote the manuscript and all authors approved the final version submitted for publication.

confocal microscopy, since NSF-induced a significant level of IgG endocytosis by Caco-2 cells. Thus, NSF-induced IgG flux was attributable to both transcytosis and the paracellular route. These data provide the first demonstration that transcytosis can be stimulated by NSF and that this was concurrent with increased paracellular permeability. Moreover, NSF with distinct architecture paired with specific substrates have the potential to provide an effective means to regulate transepithelial transport in order to optimize drug delivery.

Graphical abstract



Keywords

Nanotopography; drug delivery; epithelial permeability; calcium switch; tight junctions; transcytosis; FcRn

1. Introduction

Epithelia are composed of polarized cells that enable organs to compartmentalize. Although each epithelium is specialized, they all serve the common function of forming barriers that share common regulatory mechanisms and molecular constituents. There are two major pathways that extracellular material can use to move across an epithelial monolayer: the paracellular route which is the movement through intercellular junctions and the transcellular route which is the movement through cells [1].

The paracellular pathway involves passive diffusion between cells that is regulated by structures known as tight junctions. Tight junctions link adjacent cells and occlude the paracellular space, thus presenting a significant obstacle to delivery of macromolecules. Tight junctions are composed of transmembrane proteins (claudins, occludin) linked to the actin cytoskeleton through scaffold proteins (including zonula occludens (ZO)-1, ZO-2, and ZO-3) [2–4]. Although tight junctions can act as ion and water channels [5, 6], the paracellular permeability of larger molecules requires tight junctions to be actively opened and remodeled [7].

By contrast, the transcellular route is a barrier selective pathway that, for ions and small molecules, is mediated by specific transporters or channels located on the apical or basolateral plasma membrane [8, 9]. In the case of macromolecules, transcellular transport occurs through a process known as transcytosis that represents the coordinated internalization of ligands by receptor-mediated endocytosis followed by transit through the cell and eventual delivery to the basolateral membrane via exocytosis [10, 11].

Techniques to augment the transepithelial passage of drugs would be of great utility and are an active area of research [10, 12–17]. Measuring the flux rates of fluorescent or radiolabeled tracers is a commonly employed method to assess the ability of molecules to traverse across epithelial barriers. As generally applied, flux rates provide a relative measure of how different treatments can affect transepithelial transport [1]. Here we have extended the utility of this approach by using the calcium switch method, where cells are cultured in medium containing low calcium and normal magnesium, as a means to fully disassemble epithelial junctions while maintaining cell attachment [18, 19]. Measuring transepithelial flux in calcium-depleted cells reflects the maximum level of paracellular flux unencumbered by intercellular junctions that was then used to calibrate the relative enhancement of transepithelial transport induced by other treatments.

In this study, we examined two specific nanopatterns, Defined Nanostructure 2 (DN2) and Defined Nanostructure 3 (DN3), that were nanoimprinted on either polypropylene (PP) or polyether ether ketone (PEEK) generated from molds using electron-beam lithography [16, 17]. We previously discovered that nanostructured surfaces have the capacity to enhance the delivery of macromolecules across epithelial monolayers by an integrin-dependent pathway that activates myosin light chain kinase to increase tight junction permeability [16, 17]. The effect of NSF on transport of substrates ranging from less than 1 kDa to 900 kDa across Caco-2 human intestinal epithelial cells *in vitro* was assessed and compared to the maximum flux rate for these same substrates through fully disassembled tight junctions in calcium-depleted cells. We unexpectedly found that NSFs specifically stimulated the transport of fluorescently tagged Fab and IgG at a significantly higher rate of flux than would have been predicted based on measurements obtained with the calcium switch method, suggesting that NSFs induced an active transepithelial transport pathway. Using confocal immunofluorescence microscopy, we found that in addition to increasing paracellular flux, NSFs also stimulated transcellular transport of IgG via transcytosis. To our knowledge, this represents the first demonstration of transcytosis being stimulated through contact with a nanostructured surface. Induced transcytosis has ramifications for the use of NSFs in drug delivery devices designed to enable macromolecules to cross epithelial barriers.

2. Materials and Methods

2.1 Nanostructured thin film (NSF) fabrication

Molds for NSFs were fabricated using electron beam lithography followed by anisotropic reactive ion etching to generate small features on the nanometer length scale. Next, nanoimprint lithography was employed to imprint the nanofeatures from the nanofeatured mold onto unstructured thin films (UFs) composed of either polypropylene (PP) or polyether ether ketone (PEEK) through a stamping process [17].

2.2 Cell culture

Caco-2 cells were seeded at an initial density of 200,000 cells/cm² in the upper chamber of 6.5 mm insert Transwell (Costar; Corning Incorporated, Kennebunk, ME.) Approximately 0.25 ml of MEM (Minimum Essential Medium Eagle with Earle's salts and L-glutamine, Corning Cellgro #10-010-CV) containing 20 % Fetal Bovine Serum (FBS; Premium Select,

Atlanta Biologicals), 100 mM Sodium Pyruvate (ThermoFisher), Pen/Strep (Hyclone), Amphotericin B (Sigma) and Gentamicin (Sigma). The bottom well contained 0.5 ml MEM. The cells were incubated in a CO₂ incubator at 37°C for 5 days, with a change of medium every second day until they formed a high transepithelial resistance (TER) monolayer of 500 Ω×cm² or higher. TER was measured using a voltohmmeter (World Precision Instruments) where the measured resistance in Ohms was multiplied by the area of the Transwell filter (0.33 cm²).

2.3 Assessment of cell viability

Cell viability was measured using the Live/Dead viability/cytotoxicity kit (ThermoFisher, #L3224) [20]. Cells were washed twice with HEPES-buffered Ringer's solution (140 mM NaCl, 2 mM CaCl₂·2H₂O, 1 mM MgCl₂·6H₂O, 10 mM glucose and 10 mM NaHEPES, pH 7.3). Each well was then incubated with 100 μl of a solution containing 2 μM calcein-AM and 4 μM ethidium homodimer, in Ringer's, for 45 min at RT. The cells were then mounted on slides and immediately analyzed by fluorescence microscopy using an Olympus IX70 microscope with a U-MWIBA filter pack (BP460–490, DM505, BA515–550) or U-MNG filter pack (BP530–550, DM570, BA590–800). Alternatively, we used the MTT assay to measure cell viability. A 12mM stock solution of MTT(3-(4,5-dimethylthiazol-2-yl)-2,5-diphenyltetrazolium bromide), Invitrogen) was prepared by adding 1mL of sterile PBS to one 5mg vial of MTT. Caco-2 cells were seeded as described above were washed twice with phenol free media and then further incubated for 2 h as controls or in contact with either unstructured PEEK or DN3. The cells were then harvested and placed in a 96-well plate followed by the addition of 10 μL of 12 mM MTT stock to each well and incubated at 37°C for 4 hours. Next, 50 μL of DMSO was added to each well and mixed thoroughly with a pipette then incubated for 10 min at 37°C. Sample absorbance was read at 540nm.

2.4 Dye flux permeability assay

Probes for dye flux included: calcein (ThermoFisher # C481; 2 μg/ml); Texas Red-labeled 10 kDa dextran (ThermoFisher # D1863; 10 μg/ml); Alexa Fluor 488-labeled Donkey IgG (Jackson ImmunoResearch #711-545-152; 8.3 μg/ml); Alexa Fluor 594-labeled Donkey Fab fragment(Jackson ImmunoResearch #711-587-003; 75 μg/ml); Cy3-labeled Human IgG (Jackson ImmunoResearch #009-160-003; 8.3 μg/ml); Cy2-labeled Human serum IgA (Jackson ImmunoResearch #009-220-011; 29.4 μg/ml); and Alexa Fluor 488-labeled Human IgM (Jackson ImmunoResearch #009-540-012; 29.4 μg/ml).

Caco-2 cells were equilibrated with Ringer's solution for 30 min at 37°C and then the upper buffer was replaced with Ringers containing the probe of interest. In some cases, probes with compatible fluorophores were co-incubated to simultaneously measure flux of two different markers. Cells were then unstimulated (control) or stimulated and placed in contact with either an UF (PP, PEEK) or a NSF (DN2, DN3) as previously described [17]. Over a two hour time-course, aliquots were withdrawn from the lower chamber every 30 min and measured using a multichannel plate fluorimeter (BioTek-Synergy H Microplate Reader, Winooski, VT) set to the appropriate excitation and emission wavelengths. Absolute amounts of flux were determined using a standard curve, and plotted as the amount of

material appearing in the lower chamber of the Transwell vs. time (e.g. Figure 4). The apparent rate of diffusion was calculated using the slope of the flux curve [16, 17].

2.5 Scanning Electron Microscopy and Atomic Force Microscopy

DN2 and DN3 NSF s were directly imaged using a Phenom scanning electron microscope (SEM) and Bruker Scan Assist atomic force microscope (AFM). In addition, DN2 and DN3 NSF s in contact with Caco-2 cells on Transwells for 2 h were removed and immediately analyzed by SEM.

2.6 Calcium depletion

To deplete extracellular Ca^{2+} , confluent Caco-2 monolayers were washed once with calcium-free Eagle's MEM (Sigma, #M8167) and then incubated overnight in Calcium-free Eagle's MEM containing 10 μM CaCl_2 with supplements (L-glutamine, 10mM HEPES, Na Pyruvate, Pen/Strep) and 5% dialyzed FBS (ThermoFisher, #26400036) [21]. The cells were then washed once with calcium free Ringer's solution, incubated for 15 min at 37°C and then dye flux was measured as described above and compared with cells treated in parallel with medium containing control levels of calcium (2 mM) or empty wells that did not contain any cells.

2.7 Immunofluorescence microscopy

Cell monolayers were incubated with NSF s along with Cy3-labeled Human IgG (Jackson ImmunoResearch, #009-160-003) on 6.5 mm Transwells for 2 hr. The cells were then washed with DPBS (+ 2 mM CaCl_2 , + 1 mM MgCl_2) and fixed in 4% PFA on ice for 10 min. Cell monolayers were blocked in 0.5% Triton X for 10 min followed by another wash with DPBS. Cells were then incubated for 1 h with primary antibodies; mouse anti-ZO-1 (ThermoFisher, #33-9100) antibodies in 3% BSA overnight then incubated for 1 hr with secondary antibodies; Cy2-labeled Goat anti-mouse (Jackson ImmunoResearch, #111-225-1440). Fluorescence images were taken using an Olympus IX70 microscope with a U-MWIBA filter pack (BP460–490, DM505, BA515–550) or U-MNG filter pack (BP530–550, DM570, BA590–800). The fluorescence Z-series images were visualized using Olympus FV 1000/TIRF laser scanning confocal microscope. Images were Z-stacked using FUJI software (NIH Image J) [22].

2.8 Statistics

Statistics were calculated using GraphPad Prism 6 with one-way analysis of variance (ANOVA) where $p < 0.5$ was used as a measure of statistical significance.

3. Results

3.1 NSF s decrease barrier function without affecting viability

The overall goal of this study was to develop methods to calibrate flux measurements to determine the effect of nanostructured surfaces (NSF s) on the transepithelial permeability of a series of differently structured tracers, most of which were based on different classes of immunoglobulins.

The NSF s that we examined, DN2 and DN3, were imprinted on PP and PEEK, respectively. We first examined the fine structure of these NSF s using Scanning Electron Microscopy (SEM) and Atomic Force Microscopy (AFM) (Figure 1). DN2 consisted of a uniform array of nanopillars which each were 200 nm in width. By contrast, DN3 had three different nanopillar geometries of 200 nm, 400 nm and 1000 nm in diameter. Feature height was ~300 nm for DN2 and ranged from 80 to 370 nm for DN3. DN2 and DN3 differed in roughness where the root mean square (rms) of surface height measurements was 13.4 nm and 105 nm for DN2 and DN3, respectively [17].

Our approach was to use NSF s to stimulate the transepithelial permeability of Caco-2 cells cultured on permeable supports over a 2 h period. We previously determined that NSF s specifically increase permeability of labeled tracers in an integrin-dependent manner [16]. To determine whether there was direct contact between NSF s and epithelial cells, we examined NSF s after co-incubation with confluent monolayers of Caco-2 cells on Transwell permeable supports. As shown in Figure 1b by SEM, both DN2 and DN3 contained cell-derived membranous material after 2h of contact with Caco-2 cells. The conformation of this material differed depending on the NSF used, where low power SEM revealed larger patches of material associated with DN2 as opposed to DN3. At high power, it was revealed that DN3 had mostly small particulates associated with the largest pillars as opposed to the larger patches of material associated with DN2.

Since there was cell-derived material that remained in contact with both DN2 and DN3, we measured whether NSF s had a deleterious effect on cell viability using the Live/Dead fluorometric and MTT assays (Figure 2). UF s and NSF s did not have a significant effect on cell viability, which was comparable to unstimulated Caco-2 cells. We then examined the effect of NSF s on barrier function using transepithelial resistance (TER) to measure ion permeability [17]. Caco-2 cells grown to confluency to form high resistance monolayers showed a significant and comparable decrease in TER following 2 h incubation with either UF s or NSF s as compared with control cells treated in parallel (Figure 3). These data are consistent with previous observations that NSF s reduce epithelial barrier function while having little effect on cell viability [16, 17].

3.2 Calcium switch to measure maximum paracellular flux rates

We then systematically measured the effect of NSF s on paracellular flux of solutes with varying size and composition. While TER is a measure of instantaneous transcellular permeability to ions that occurs on a microsecond timescale, paracellular flux of solutes occurs over a time scale of minutes to hours and thus these two measures are not necessarily concordant [23]. We were particularly interested in comparing whether NSF s induce paracellular flux rates that were comparable to that of fully disassembled tight junctions representing a completely unobscured path between cells. To do this, we developed a novel approach based on the calcium switch assay, where flux was quantified across cells incubated overnight in low calcium, but in the presence of normal magnesium to have fully disassembled junctions [24]. As shown in Figure 4a-f, Caco-2 cells showed significant increases in the paracellular flux of tracers ranging in size from 0.62 kDa (calcein) and 10 kDa (Texas Red dextran) to 900 kDa (IgM). Using the slope of these curves, we were able to

calculate the paracellular diffusion constant for macromolecule probes and found that there was an inverse relationship between probe mass and paracellular diffusion coefficient between calcium-depleted cells (Figure 4g). Although the small molecule calcein potentially has access to the subjunctional reticulum that excludes macromolecules including dextrans [25], it still had a much higher apparent diffusion coefficient relative to the other probes examined, both for calcium-depleted and control cells. Note that two comparably sized probes (IgG and IgA) had comparable paracellular diffusion coefficients in the calcium switch assay (Figure 4d,e). Also, paracellular diffusion for cells in either normal (2 mM) or low calcium (10 μ M) was dramatically lower than that measured for empty wells that did not contain cells (Supplemental Figure S1), consistent with the presence of cells in the Transwells impeding the free diffusion of tracers regardless of whether they had intact junctions or not.

3.3 NSF-stimulated transcellular flux differentially affects different tracers

We used the paracellular diffusion coefficient of cells in low calcium as a measure of “maximum” paracellular flux by an unobscured path through fully disassembled tight junctions. This enabled us to normalize flux data obtained from cells that were stimulated with UFs or NSFs. First, cells were grown to form confluent high resistance monolayers. Then, different probes were added to the top chamber in HEPES-buffered Ringer’s containing normal calcium concentration, cells were placed in contact with a UF or NSF, and then paracellular flux was measured over a 2 h time course. The diffusion coefficient induced by UFs or NSFs was calculated and normalized to flux rates measured from cells in low calcium (Figure 4). Probes investigated were calcein (0.62 kDa), Texas Red Dextran (10k Da), Fab fragments (55 kDa), intact IgG (160 kDa), serum IgA (180 kDa) and IgM (900 kDa).

We found that there were probe-dependent differences in the ability of UFs and NSFs to stimulate transepithelial flux (Figure 5). The most dramatic effect was on IgG (Figure 5d), which showed a 10-20 fold higher rate of flux in response to UFs and NSFs as compared with the flux rate for unstimulated cells. DN2 and DN3 were more effective at stimulating IgG flux as opposed to PP and PEEK, although the UFs also enhanced IgG flux. Critically, the flux rate for IgG was significantly enhanced over that observed for cells in low calcium, i.e. greater than the maximum rate predicted if only the paracellular route was used. This suggests that UFs and NSFs stimulated an active transport pathway by direct contact. Fab fragments (Figure 5c) showed a trend that was similar to IgG although it was lower in magnitude. Interestingly, IgA, which is comparable in size to IgG, was much less sensitive to NSF stimulation (Figure 5e,g,h), suggesting that an IgG-specific transcellular pathway was being stimulated by NSFs. This was confirmed using cells that were simultaneously probed with IgG and IgA where the relative flux of IgG was greater than that of IgA (Figure 5i). Neither UFs nor NSFs showed statistically significant enhancement of calcein and Texas Red Dextran flux when assessed over a 2 h period (Figure 5a,b). However, UFs and NSFs consistently showed a flux rate for calcein and Texas Red Dextran that trended to be about double that of unstimulated cells. PEEK and DN3 did significantly stimulate flux of IgM ~3-fold higher than unstimulated cells (Figure 5f).

3.4 NSF s induce IgG transcytosis

The specific enrichment of IgG flux by NSF s suggested activation of a transcellular pathway, most likely transcytosis. To determine whether this is the case we examined transport of Cy3-labeled IgG by Caco-2 cells stimulated with either DN2 or DN3 by confocal immunofluorescence microscopy. As shown in Figure 6, both of these NSF s induced intracellular localization of IgG that did not overlap with the tight junction marker ZO-1. By contrast, there was little, if any IgG associated with unstimulated cells. Note that for NSF-stimulated cells, ZO-1 showed the characteristic ruffling pattern previously observed [17]. By morphometric analysis, we found that the majority of cell-associated IgG did not co-localize with ZO-1, where $76.3 \pm 1.8 \%$ (n=5) of IgG was intracellular for DN2 stimulated cells and $61.3 \pm 10.2 \%$ (n=5) of IgG was intracellular for DN3 stimulated cells. However, some Cy3-IgG was junction localized as well (Figure 6b). Taken together, these data support a model where contact of NSF s with an epithelial monolayer has the capacity to promote transepithelial flux of macromolecules through both the paracellular and transcellular pathways.

4. Discussion

Here we demonstrate for the first time that NSF s stimulate transcytosis, as well as increase paracellular flux. There were two keys to determining that this was the case, 1) using a series of immunoglobulin-based fluorescent tracers of different size and composition (Figure 5) and 2) using calcium-depleted cells to measure the maximum level of paracellular flux in epithelial cells where the tight junctions were fully disassembled (Figure 4). Two different NSF s, DN2 and DN3, imprinted on two different substrates, PP and PEEK, had comparable effects where DN2 and PP generally were more effective at promoting transepithelial flux of IgG than DN3 and PEEK. NSF s were generally more effective at stimulating transepithelial transport than UF s, consistent with the importance of a nanostructured surface in stimulating the epithelium [16, 17].

Our findings support the use of NSF s as a new approach for the simultaneous enhancement of paracellular and transcellular drug transport that is particularly effective for immunoglobulin-based therapeutics. Several classes of macromolecular pharmaceutical agents, such as adalimumab and etanercept, are either engineered antibodies or chimeric proteins containing the Fc portion of IgG which promotes their efficacy through specific targeting and by decreasing rates of clearance [15, 26–29]. That IgG transport was significantly more enhanced than transport of IgA or Fab supports the hypothesis that antibody binding to so-called epithelial neonatal Fc receptors (FcRn) was an important part of NSF-stimulated transport mediated by substrate endocytosis and subsequently transcytosis [11, 30, 31]. FcRn is broadly expressed by adult epithelia and so is an appealing target for macromolecular therapeutics. Interestingly, a low-affinity IgA receptor has been reported to be expressed by intestinal epithelial cells, specifically colonic cells that may explain our observations that NSF s stimulate IgA flux, albeit to a lesser extent than IgG [32].

In addition to binding to Fc regions from multiple species, FcRn also has been shown to bind albumin and mediate its endocytosis [11, 33]. Our previous results also demonstrated

enhanced transepithelial flux of fluorescently-labeled albumin induced by NSF s [16, 17] are thus consistent with the findings here that NSF s also stimulate IgG transcytosis.

NSF s also increased paracellular flux as well as transcytosis, as evidenced by decreased TER (Figure 3). We also observed hallmark changes in tight junction morphology in ZO-1 (Figure 6a), which had a ruffled pattern as previously described [16, 17]. That transepithelial flux under some circumstances was comparable to the level observed for calcium depleted cells (e.g. PP-induced Fab transport) suggests transit through the paracellular route may predominate in that instance. Our previous study indicated that the paracellular route was the major pathway for NSF-stimulated transport of fluorescently tagged IgG [17]. However, in that instance, the NSF used to promote flux was P(1.5) which has features significantly higher than either DN2 or DN3 used here. Also, in that study, cells were incubated with >10-fold more IgG than in the present study (100 µg/ml vs. 8.3 µg/ml), so it is likely that under those conditions, transport through FcRn and the transcytotic pathway were saturated [29], thus favoring paracellular transport.

SEM analysis of DN2 and DN3 after incubation with cells demonstrated that there was cell associated material attached to the NSF s (Figure 1). This suggests that NSF s were in direct contact with the cells and is consistent with our previous observation that the effects of NSF s on transepithelial flux were antagonized by integrin-blocking peptides [16]. The nature of NSF-attached material is not known at present. Since NSF s do not have an adverse effect on cell viability (Figure 2), NSF-associated material is unlikely to represent fragments derived from damaged cells. One possibility is that exosomes or nanotubes produced in response to NSF contact remain associated with the films [34]. Whether this is the case or whether NSF-associated material has some other origin remains to be determined.

We took advantage of the calcium switch method as a means to disassemble tight junctions to develop a novel method for measuring maximum paracellular flux [21, 35–38]. By maintaining cells in calcium-deficient medium, this allowed the tight junctions to remain open to provide a measure paracellular flux through an unencumbered path. Note that magnesium concentration was maintained at normal levels that enabled the cells to remain attached to the cell substrate. By and large paracellular flux of macromolecules between calcium-depleted cells showed size dependent differences in flux, with decreased paracellular diffusion correlating with increased mass of the probe examined.

The transport of smaller molecules, 0.62 kDa calcein and 10 kDa Texas Red Dextran, was less enhanced by NSF s than macromolecules, consistent with previous studies [17]. There also was a size restriction for this effect as well, since NSF-stimulation of IgM was modest and restricted to DN3 and PEEK. Other molecular properties important for drug pharmacokinetics include charge and lipophilicity that can also influence transepithelial flux [39]. By examining a series of probes based on immunoglobulins, we were able to identify another aspect that influences flux, namely physiologic interactions between these probes and cells, in this case, FcRn receptors. Whether NSF s specifically stimulate FcRn activity or more broadly influence transcytosis in addition to promoting paracellular flux remains to be determined.

Transdermal, subcutaneous and oral delivery of pharmaceutical agents is the current standard of care [40, 41]. However each of these methods is not well suited to macromolecular agents. For instance, agents such as the biopharmaceutical IgG protein adalimumab must be administered by bolus subcutaneous or intramuscular injection that is difficult to control and painful to administer [40]. Our findings here demonstrated that NSFs are particularly effective in stimulating transepithelial IgG transport by both the paracellular route and by transcytosis. This underscores the potential utility of different nanopatterns, film compositions, and substrates as a means to optimize movement of macromolecular therapeutic agents through epithelial barriers.

Supplementary Material

Refer to Web version on PubMed Central for supplementary material.

Acknowledgments

We thank members of the Desai and Koval labs for critical reading of the manuscript. Funding for this work was provided by National Institutes of Health R01-EB018842, U54-CA118638, R25-GM058268, G12-MD007602 and Kimberly-Clark Corporation. This research project was supported in part by the Emory University Integrated Cellular Imaging Microscopy Core.

References

1. Koval, M. Structure and Function of Epithelial and Endothelial Barriers. In: Muro, S., editor. Drug Delivery Across Physiological Barriers. CRC Press; Boca Raton FL: 2016. p. 3-40.
2. Van Itallie CM, Anderson JM. Architecture of tight junctions and principles of molecular composition. *Semin Cell Dev Biol.* 2014; 36C:157–165.
3. Tsukita S, Furuse M, Itoh M. Multifunctional strands in tight junctions. *Nat Rev Mol Cell Biol.* 2001; 2:285–293. [PubMed: 11283726]
4. Ivanov AI, Parkos CA, Nusrat A. Cytoskeletal regulation of epithelial barrier function during inflammation. *Am J Pathol.* 2010; 177:512–524. [PubMed: 20581053]
5. Suzuki H, Nishizawa T, Tani K, Yamazaki Y, Tamura A, Ishitani R, Dohmae N, Tsukita S, Nureki O, Fujiyoshi Y. Crystal structure of a claudin provides insight into the architecture of tight junctions. *Science.* 2014; 344:304–307. [PubMed: 24744376]
6. Shen L, Weber CR, Raleigh DR, Yu D, Turner JR. Tight junction pore and leak pathways: a dynamic duo. *Annu Rev Physiol.* 2011; 73:283–309. [PubMed: 20936941]
7. Schneeberger EE, Lynch RD. The tight junction: a multifunctional complex. *Am J Physiol Cell Physiol.* 2004; 286:C1213–1228. [PubMed: 15151915]
8. Venkatasubramanian J, Ao M, Rao MC. Ion transport in the small intestine. *Curr Opin Gastroenterol.* 2010; 26:123–128. [PubMed: 20010100]
9. Eaton DC, Helms MN, Koval M, Bao HF, Jain L. The contribution of epithelial sodium channels to alveolar function in health and disease. *Annu Rev Physiol.* 2009; 71:403–423. [PubMed: 18831683]
10. Tuma PL, Hubbard AL. Transcytosis: crossing cellular barriers. *Physiol Rev.* 2003; 83:871–932. [PubMed: 12843411]
11. Martins JP, Kennedy PJ, Santos HA, Barrias C, Sarmiento B. A comprehensive review of the neonatal Fc receptor and its application in drug delivery. *Pharmacol Ther.* 2016; 161:22–39. [PubMed: 27016466]
12. Salama NN, Eddington ND, Fasano A. Tight junction modulation and its relationship to drug delivery. *Adv Drug Deliv Rev.* 2006; 58:15–28. [PubMed: 16517003]
13. Lemmer HJ, Hamman JH. Paracellular drug absorption enhancement through tight junction modulation. *Expert Opin Drug Deliv.* 2013; 10:103–114. [PubMed: 23163247]

14. Collett A, Sims E, Walker D, He YL, Ayrton J, Rowland M, Warhurst G. Comparison of HT29-18-C1 and Caco-2 cell lines as models for studying intestinal paracellular drug absorption. *Pharm Res.* 1996; 13:216–221. [PubMed: 8932439]
15. Rath T, Baker K, Dumont JA, Peters RT, Jiang H, Qiao SW, Lencer WI, Pierce GF, Blumberg RS. Fc-fusion proteins and FcRn: structural insights for longer-lasting and more effective therapeutics. *Crit Rev Biotechnol.* 2015; 35:235–254. [PubMed: 24156398]
16. Walsh L, Ryu J, Bock S, Koval M, Mauro T, Ross R, Desai T. Nanotopography facilitates in vivo transdermal delivery of high molecular weight therapeutics through an integrin-dependent mechanism. *Nano Lett.* 2015; 15:2434–2441. [PubMed: 25790174]
17. Kam KR, Walsh LA, Bock SM, Koval M, Fischer KE, Ross RF, Desai TA. Nanostructure-mediated transport of biologics across epithelial tissue: enhancing permeability via nanotopography. *Nano Lett.* 2013; 13:164–171. [PubMed: 23186530]
18. Gumbiner B, Stevenson B, Grimaldi A. The role of the cell adhesion molecule uvomorulin in the formation and maintenance of the epithelial junctional complex. *J Cell Biol.* 1988; 107:1575–1587. [PubMed: 3049625]
19. Capaldo CT, Nusrat A. Cytokine regulation of tight junctions. *Biochim Biophys Acta.* 2009; 1788:864–871. [PubMed: 18952050]
20. Muro S, Cui X, Gajewski C, Murciano JC, Muzykantov VR, Koval M. Slow intracellular trafficking of catalase nanoparticles targeted to ICAM-1 protects endothelial cells from oxidative stress. *Am J Physiol Cell Physiol.* 2003; 285:C1339–1347. [PubMed: 12878488]
21. Ivanov AI, Hunt D, Utech M, Nusrat A, Parkos CA. Differential roles for actin polymerization and a myosin II motor in assembly of the epithelial apical junctional complex. *Mol Biol Cell.* 2005; 16:2636–2650. [PubMed: 15800060]
22. Schlingmann B, Overgaard CE, Molina SA, Lynn KS, Mitchell LA, Dorsainvil White S, Matheyses AL, Guidot DM, Capaldo CT, Koval M. Regulation of claudin / zonula occludens-1 complexes by hetero-claudin interactions. *Nat Commun.* 2016; 7:12276. [PubMed: 27452368]
23. Koval M. Claudin heterogeneity and control of lung tight junctions. *Annu Rev Physiol.* 2013; 75:551–567. [PubMed: 23072447]
24. Ivanov AI, McCall IC, Parkos CA, Nusrat A. Role for Actin Filament Turnover and a Myosin II Motor in Cytoskeleton-driven Disassembly of the Epithelial Apical Junctional Complex. *Mol Biol Cell.* 2004; 15:2639–2651. [PubMed: 15047870]
25. Mamdough Z, Chen X, Pierini LM, Maxfield FR, Muller WA. Targeted recycling of PECAM from endothelial surface-connected compartments during diapedesis. *Nature.* 2003; 421:748–753. [PubMed: 12610627]
26. Taylor PC. Pharmacology of TNF blockade in rheumatoid arthritis and other chronic inflammatory diseases. *Curr Opin Pharmacol.* 2010; 10:308–315. [PubMed: 20172761]
27. Weir AN, Nesbitt A, Chapman AP, Popplewell AG, Antoniw P, Lawson AD. Formatting antibody fragments to mediate specific therapeutic functions. *Biochem Soc Trans.* 2002; 30:512–516. [PubMed: 12196125]
28. Vincent KJ, Zurini M. Current strategies in antibody engineering: Fc engineering and pH-dependent antigen binding, bispecific antibodies and antibody drug conjugates. *Biotechnol J.* 2012; 7:1444–1450. [PubMed: 23125076]
29. Ternant D, Paintaud G. Pharmacokinetics and concentration-effect relationships of therapeutic monoclonal antibodies and fusion proteins. *Expert Opin Biol Ther.* 2005; 5(Suppl 1):S37–47. [PubMed: 16187939]
30. Suzuki T, Ishii-Watabe A, Tada M, Kobayashi T, Kanayasu-Toyoda T, Kawanishi T, Yamaguchi T. Importance of neonatal FcR in regulating the serum half-life of therapeutic proteins containing the Fc domain of human IgG1: a comparative study of the affinity of monoclonal antibodies and Fc-fusion proteins to human neonatal FcR. *J Immunol.* 2010; 184:1968–1976. [PubMed: 20083659]
31. Kuo TT, Aveson VG. Neonatal Fc receptor and IgG-based therapeutics. *MAbs.* 2011; 3:422–430. [PubMed: 22048693]
32. Kitamura T, Garofalo RP, Kamijo A, Hammond DK, Oka JA, Caflisch CR, Shenoy M, Casola A, Weigel PH, Goldblum RM. Human intestinal epithelial cells express a novel receptor for IgA. *J Immunol.* 2000; 164:5029–5034. [PubMed: 10799857]

33. Sleep D, Cameron J, Evans LR. Albumin as a versatile platform for drug half-life extension. *Biochim Biophys Acta*. 2013; 1830:5526–5534. [PubMed: 23639804]
34. Belting M, Witttrup A. Nanotubes, exosomes, and nucleic acid-binding peptides provide novel mechanisms of intercellular communication in eukaryotic cells: implications in health and disease. *J Cell Biol*. 2008; 183:1187–1191. [PubMed: 19103810]
35. Stuart RO, Sun A, Panichas M, Hebert SC, Brenner BM, Nigam SK. Critical role for intracellular calcium in tight junction biogenesis. *J Cell Physiol*. 1994; 159:423–433. [PubMed: 8188760]
36. Saha C, Nigam SK, Denker BM. Expanding role of G proteins in tight junction regulation: α (s) stimulates TJ assembly. *Biochem Biophys Res Commun*. 2001; 285:250–256. [PubMed: 11444833]
37. Hopkins AM, Walsh SV, Verkade P, Boquet P, Nusrat A. Constitutive activation of Rho proteins by CNF-1 influences tight junction structure and epithelial barrier function. *J Cell Sci*. 2003; 116:725–742. [PubMed: 12538773]
38. Denker BM, Saha C, Khawaja S, Nigam SK. Involvement of a heterotrimeric G protein alpha subunit in tight junction biogenesis. *J Biol Chem*. 1996; 271:25750–25753. [PubMed: 8824202]
39. Arnott JA, Planey SL. The influence of lipophilicity in drug discovery and design. *Expert Opin Drug Discov*. 2012; 7:863–875. [PubMed: 22992175]
40. Mitragotri S, Burke PA, Langer R. Overcoming the challenges in administering biopharmaceuticals: formulation and delivery strategies. *Nat Rev Drug Discov*. 2014; 13:655–672. [PubMed: 25103255]
41. Sastry SV, Nyshadham JR, Fix JA. Recent technological advances in oral drug delivery – a review. *Pharm Sci Technolo Today*. 2000; 3:138–145. [PubMed: 10754543]

Highlights

- Contact of epithelial cells with nanostructured surfaces enhances transepithelial flux of soluble tracers
- The calcium switch method enables maximum paracellular flux rates across an epithelial monolayer to be measured
- Two distinct nanostructures simultaneously stimulate both transcytosis and paracellular diffusion of IgG

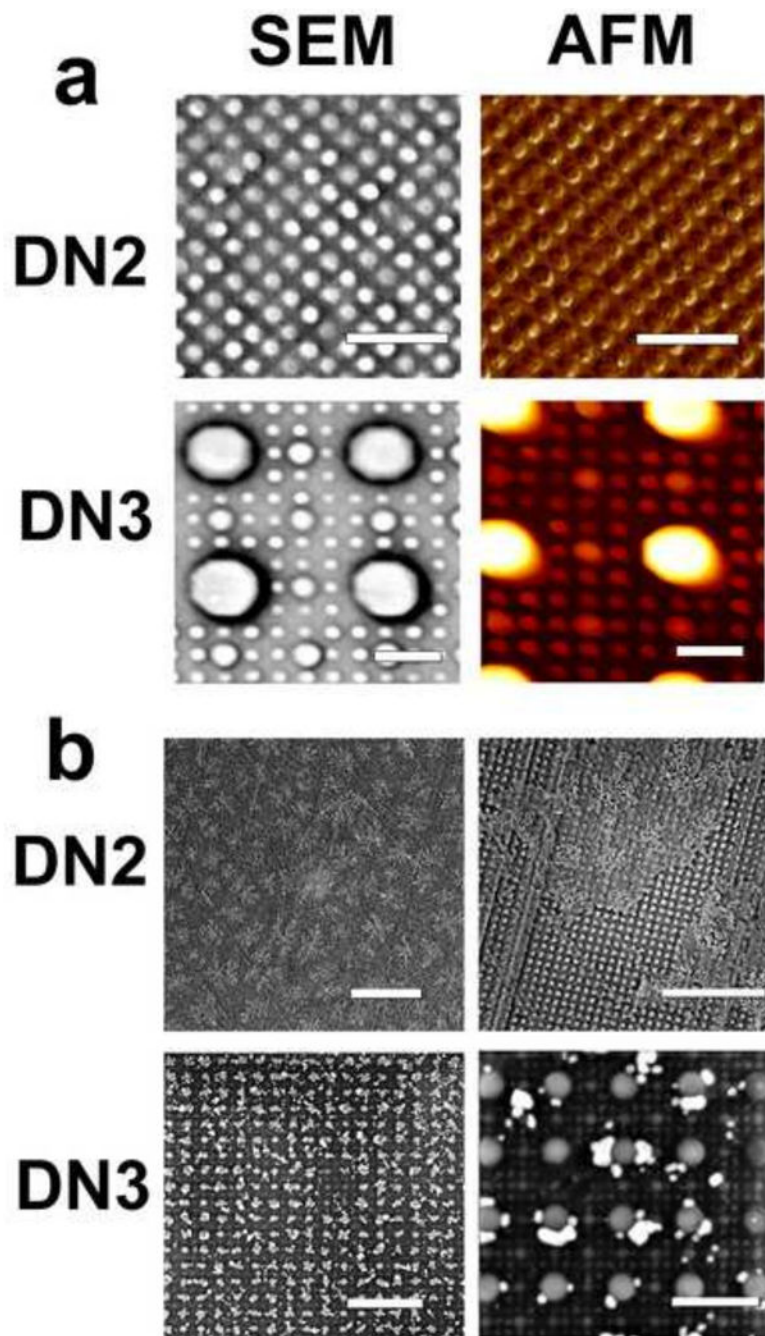


Figure 1. Scanning electron microscopy (SEM) and Atomic Force microscopy (AFM) images of nanostructured thin films (NSFs)
 (a) Nanopillar features of Defined Nanostructure 2 (DN2) on polypropylene (PP) and Defined Nanostructure 3 (DN3) on polyetheretherketone (PEEK). For DN2, the height and width of the each individual nanopillar feature is 200 nm. For DN3, there are three different nanopillar features (200 nm, 400 nm, 1000nm). Bar = 1 micron. (b) SEM images of DN2 and DN3 films removed after 2 h of contact on Caco-2 cells. Cell derived material remained adherent to the NSF surfaces in both cases. Left panels, bar = 10 microns; right panels, bar = 3 microns.

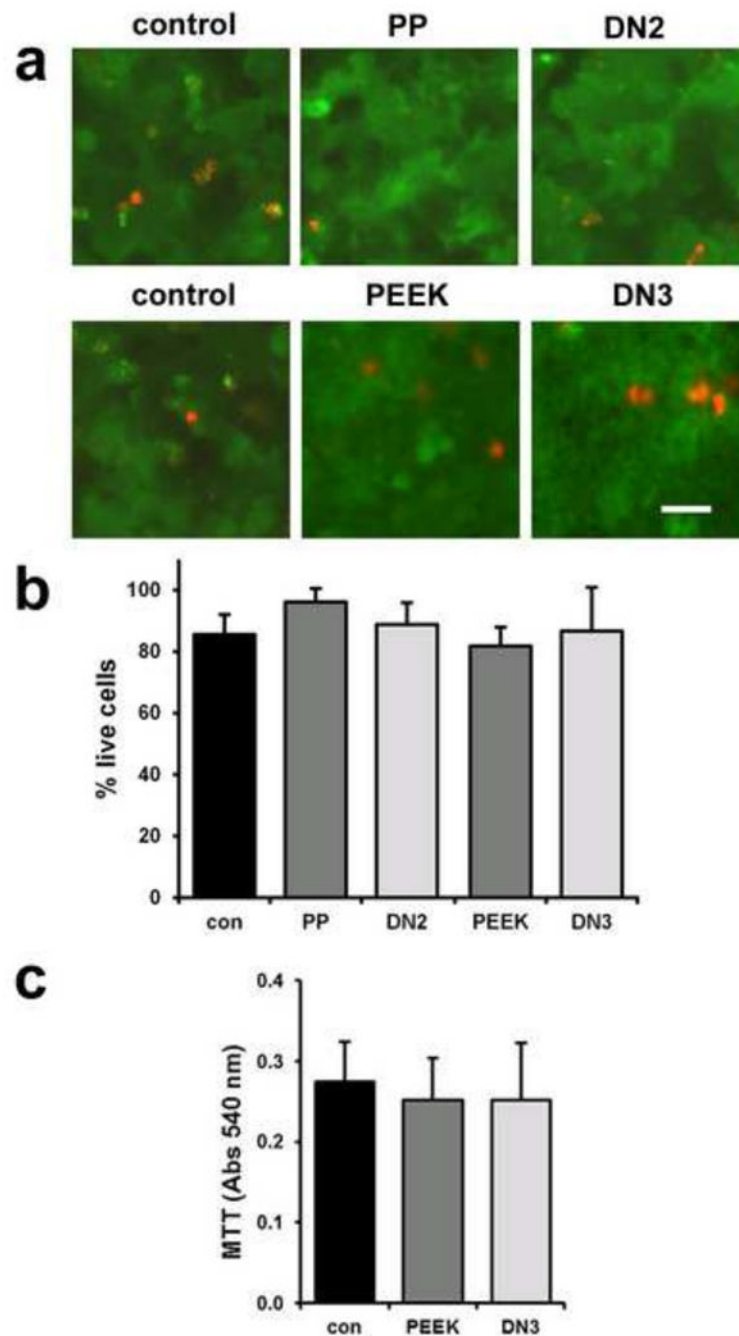


Figure 2. Nanostructured films have no effect on Caco-2 cell viability

(a) Caco-2 cells in Transwell permeable supports were either untreated (control) or were incubated for 2 h with either unstructured PP, DN2, unstructured PEEK or DN3. Cells were then analyzed using the live/dead assay where live cells are labeled with calcein-AM, (green) and dead cells are labeled with EthD-1 (red). Two different control images are presented. Bar = 10 microns. (b) Quantitation of Live/Dead labelling represented as % live cells. (c) Quantitation of cell viability using the MTT assay. For (b) and (c), data represent the mean \pm SD of three separate experiments examining the effects of UFs and NSFs on

cells from different cultures. There were no significant differences in cell viability between untreated cells and cells in contact with different surfaces.

Author Manuscript

Author Manuscript

Author Manuscript

Author Manuscript

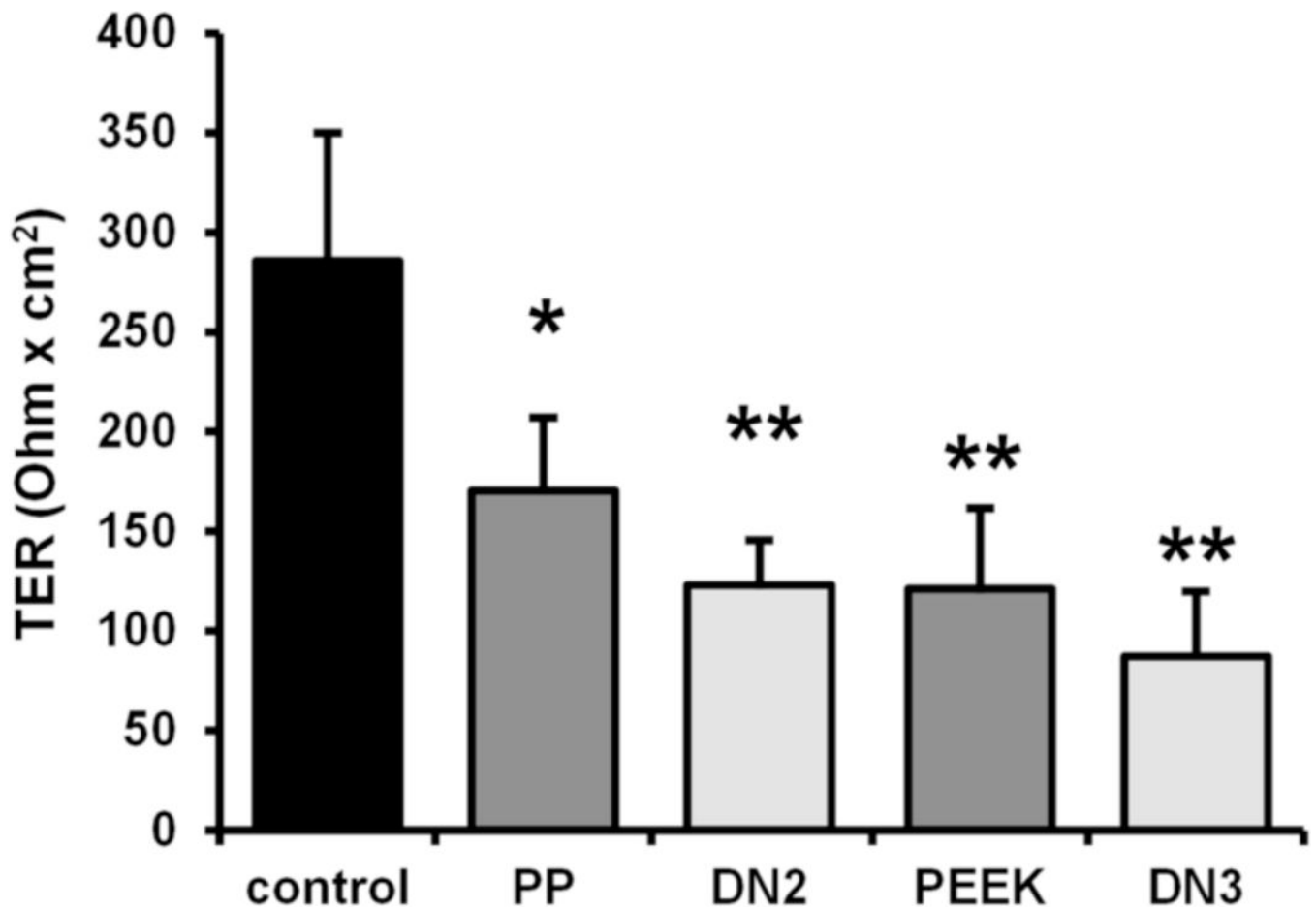


Figure 3. Nanostructured films decrease transepithelial resistance (TER)

TER of Caco-2 cells in Transwell permeable supports was measured and then the cells were either untreated (control) or were incubated for 2 h with either unstructured PP, DN2, unstructured PEEK or DN3. TER was measured again and shown as Ohm \times cm². In each case, TER was significantly lower in response to substrate contact as opposed to unchallenged cells, indicating an increase in paracellular permeability. PP, * $p=0.0011$; DN2, PEEK, DN3, ** $p<0.0001$ (mean + SD, $n=8-12$, one-way ANOVA).

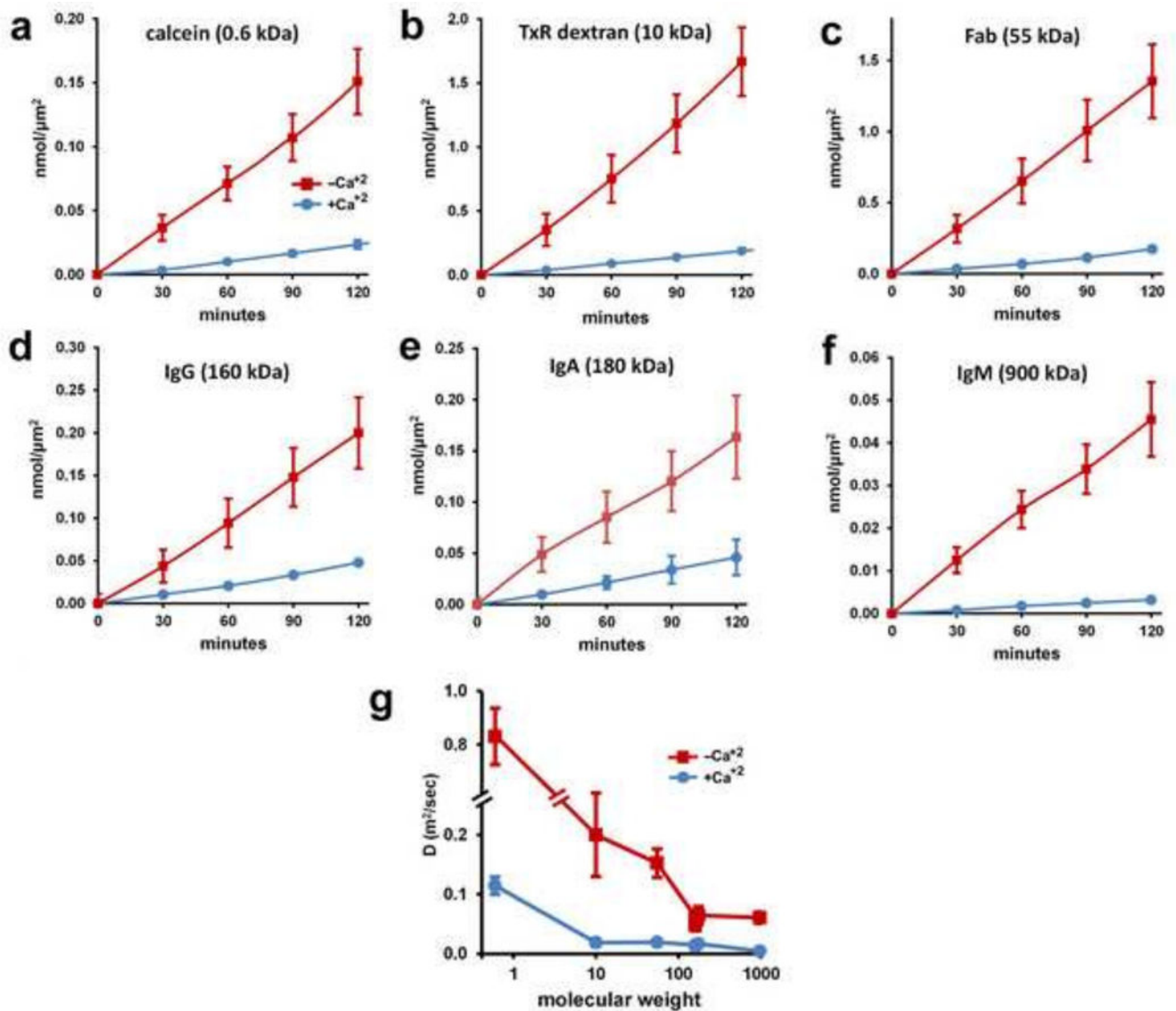


Figure 4. Calcium depletion to measure maximum paracellular permeability in otherwise unchallenged cells

(a–f) Caco-2 cells were grown to confluence on Transwell permeable supports and then incubated overnight in normal culture medium (blue) or switched to a calcium-deficient medium (red). The cells were then incubated with either calcein (a), 10 kDa Texas Red-labeled dextran (b), Fab (c), IgG (d), serum IgA (e) or IgM (f) and paracellular flux was measured. In each case, calcium depleted cells showed an increase in flux, indicating the maximum level of paracellular flux for each tracer molecule. (g) Paracellular diffusion coefficients (D) were derived from the slope of the curves in a–f and plotted as a function of tracer molecular weight. There was a decrease in paracellular fusion as a function of tracer size. Note that the comparably sized IgG and IgA-based tracers overlap in this plot. Flux measurements obtained using empty Transwells that did not contain cells were much higher than either normal or calcium-depleted cells (Supplemental Figure S1).

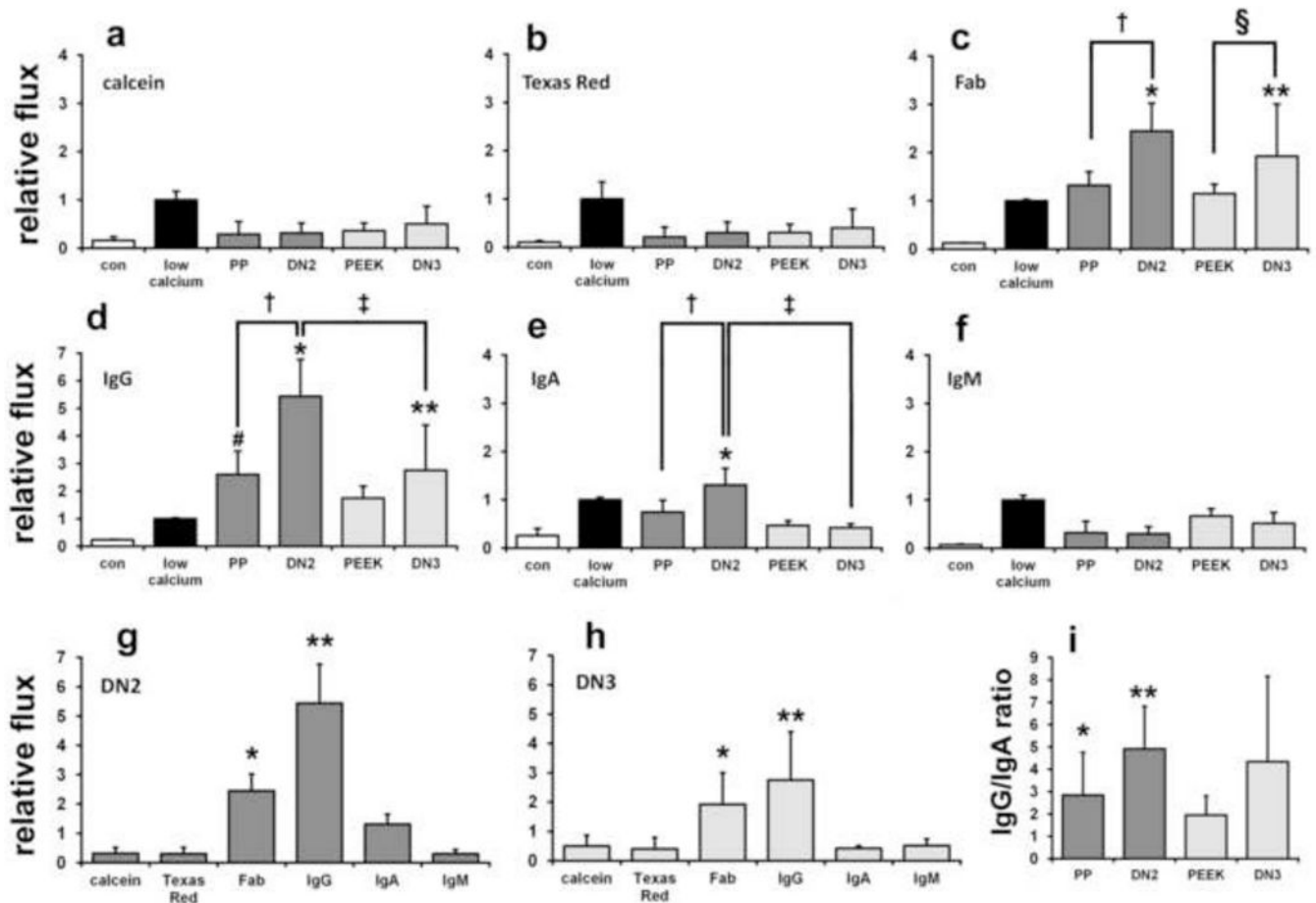


Figure 5. Differential enhancement of permeability by nanostructured films

(a–f) Caco-2 cells were grown to confluence on Transwell permeable supports, then were either untreated controls (con) or were incubated for 2 h in normal calcium containing medium with either unstructured PP, DN2 NSF, unstructured PEEK or DN3 NSF. Paracellular flux was assessed with either calcein (a), 10 kDa Texas Red-labeled dextran (b), Fab (c), IgG (d), serum IgA (e) or IgM (f). Values were then normalized to flux values obtained for unchallenged cells in low calcium, considered to represent maximum paracellular diffusion through opened tight junctions (Figure 4). For Fab, IgG and IgA, DN2 stimulated flux significantly more than unstructured PP (†) or maximum paracellular flux (*; n=6–12, all p values are in Supplementary Table S1). PP also stimulated IgG flux at a rate greater than would be predicted from cells in low calcium (#). DN3 stimulated flux of Fab and IgG significantly higher than maximum paracellular flux as well (**), as well as higher than unstructured PEEK (§), but had little effect on IgA. DN2 was also more effective than DN3 at stimulating flux of Fab and IgG (‡). (g,h) Flux rates for different substrates were compared with each other. Stimulation of Fab (*) and IgG (**) flux by DN2 and DN3 was significantly greater than that of the other tracers examined (p values in Supplementary Table S2). (i) We also examined the relative flux of hIgG and hIgA simultaneously applied to cells stimulated with unstructured films and NSFs. Stimulation of IgG flux by PP and

DN2 significantly higher than that of IgA (*p=0.0351; **p=0.004; n=4). All data represent mean + SD and significance determined by one-way ANOVA.

Author Manuscript

Author Manuscript

Author Manuscript

Author Manuscript

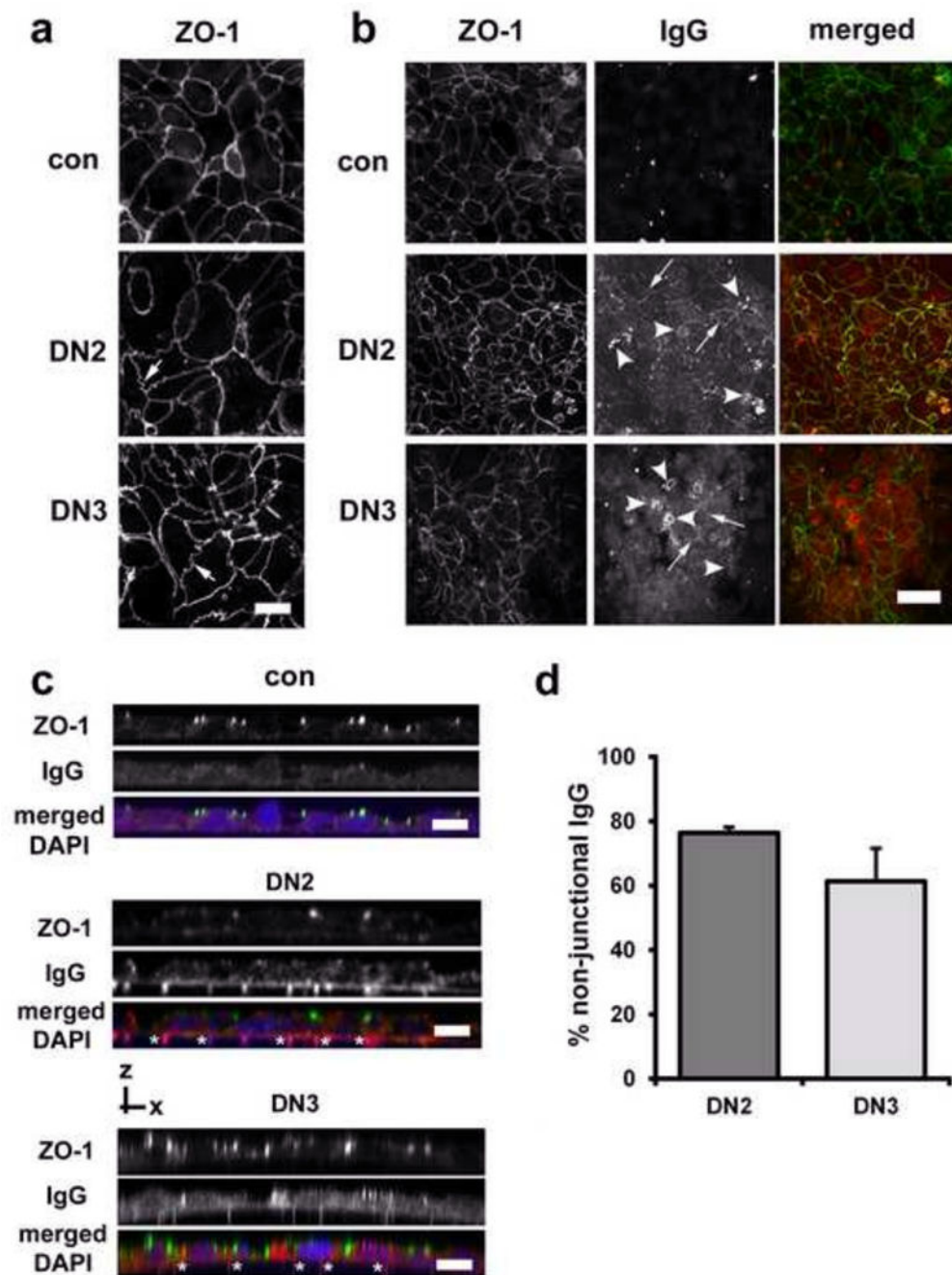


Figure 6. Nanostructured Films Induce Human IgG Endocytosis

Caco-2 cells were grown to confluence in Transwell permeable supports, then incubated for 2 h as unstimulated controls or with either DN2 or DN3 along with Cy3-labeled IgG as a tracer. The cells were then fixed, processed for confocal immunofluorescence microscopy, and labeled for the tight junction protein zonula occludens 1 (ZO-1; green). (a) High magnification images show NSF induction of ZO-1 remodeling (arrows) in a serpentine morphology that was not present in unstimulated cells (con). (b) There was an increase in red punctate labeling inside the cells treated with either of the NSFs consistent with IgG

endocytosis. Bar = 20 microns. (c) x-z projections of the cells imaged in (b) confirmed the intracellular localization of IgG below ZO-1 labeled tight junctions. In these images DAPI stained nuclei (blue) are also shown. Bar = 10 microns. (d) The relative amount of cell associated Cy3-IgG that did not co-localize with ZO-1 was quantified to determine the percent non-junctional IgG. For both DN2 and DN3, the majority of IgG was intracellular as opposed to junctional (mean + SD, n=5). This suggests that NSF's stimulate IgG endocytosis and that transcytosis contributes to transcellular flux of IgG.

Author Manuscript

Author Manuscript

Author Manuscript

Author Manuscript